Hybrid Finite Element-Modal Analysis of Jet Engine Inlet Scattering

Daniel C. Ross, John L. Volakis and Hristos T. Anastassiu

Radiation Laboratory
University of Michigan
Ann Arbor MI 48109-2122

abstract -- With the goal of characterizing jet engine inlets, a hybrid finite element-modal formulation is presented for the analysis of cavities with complex terminations. The finite element method is used to find the generalized scattering matrix for an N-port representation of the complex termination, where N is the number of traveling modes in the cavity. The cavity is assumed to be circular at the termination (engine) but the remainder of the cavity can be of arbitrary cross section. The scattered fields are obtained by tracing the fields back out of the cavity via a high frequency or modal technique with the generalized scattering matrix used in determining the fields at an aperture near the irregular cavity termination. "Proof of concept" results are presented and several issues relating to the implementation of the FEM are addressed. Among these, a new artificial absorber is developed for terminating the FEM mesh and the suitability of edge or node based elements is examined.

1.0 Introduction

The simulation of radar scattering from jet engine inlets is an important step towards the characterization of aircraft structures. While high frequency techniques can accurately simulate many scattering mechanisms on a typical aircraft, these techniques are not suitable for resonant or guiding structures such as antennas/radomes and jet engine inlets. The engine face is an intricate target, possessing complex geometrical features at the wavelength level or less, and is therefore inappropriate for high frequency analysis, By comparison, the finite element method (FEM) [1][2] is well suited for the analysis of geometrically complex, inhomogeneous volumetric targets such as the engine face. However, in spite of its inherent O(n) storage demand, the FEM analysis would still require prohibitive computational resources were it to be also used for modeling the volume enclosed by the inlet leading to the engine. To overcome this difficulty, in this report we describe a new hybrid finite element method for the analysis of the inlet-engine configuration.

The proposed hybrid FEM was originally proposed in [3]and combines ray techniques (for propogating the field to and from the engine face) and the FEM (for computing the fields scattered from the engine face). Figure 1 shows the regions to be characterized either by the finite element method or some high frequency technique. Obviously, the high frequency method is best suited for modeling the fields in the large cavity region between the inlet mouth and the engine face. Any of the well known ray methods such as the shooting and bouncing ray (SBR) [4], the generalized ray expansion (GRE) [5]or even a modal decomposition technique can be used for coupling the fields into the inlet region and guiding them from the inlet mouth to the engine face. The same ray or modal technique can also be used for propagating the fields scattered by the engine back out of the inlet.

Of importance in this analysis is the interface between the ray/modal and FEM methods, and the truncation of the finite element mesh. Given that the inlet cross section near and at the engine location is circular, and our desire to propose an efficient and flexible coupling scheme, the coupling of the FEM and ray fields in this report is accomplished via the generalized modal scattering matrix. That is, the FEM analysis generates the modal scattering matrix which can then be interfaced with any high frequency technique for computing the engine scattered fields without reference to the geometry of the jet engine. Regarding the truncation of the FEM mesh, several schemes are considered including absorbing boundary conditions, the unimoment method and a new artificial broadband absorber, with the later found most effective for this application.

The report begins with a section describing the proposed hybrid FEM method, termed as the FEM-modal method because it generates the modal scattering matrix. This section describes the role of the modal scattering matrix for interfacing with the FEM and ray techniques used for propagating the fields to and from the engine face. The next sections discuss implementation issues of the FEM technique including shape functions, application of boundary conditions and truncation of the FEM mesh. Finally, results are presented for three different inlet terminations. These terminations are rather simple and serve to validate the proposed hybrid FEM-modal methods since reference calculations using different techniques are available. Given that the emphasis of the report is on the development of the FEM-modal technique and not on the inlet field propagator, calculations refer to straight circular inlets. However, the inherent flexibility of the generalized scattering matrix allows the characterization of the same inlet terminations connected to different inlet geometries.

2.0 Finite Element-Modal Formulation

Consider the three-dimensional cavity configuration shown in Figure 1. The cavity is excited by an arbitrary field (typically a plane wave) through its opening at the left side and is assumed to have a complex geometrical configuration (an engine) at its right end. We are interested in computing the field scattered by this complex cavity termination due to a given excitation which is assumed to be specified at the left pinioning of the cavity. In our analysis, the cross section of the cavity is assumed to be arbitrary and of diameter greater than a free space wavelength up to the connectivity boundary as shown in Figure 1. Beyond this connectivity boundary, the cavity's outer perimeter is assumed to be circular but may enclose complex geometrical configurations such as an engine.

In accordance with the proposed hybrid FEM-modal formulation, the fields entering the left opening of the inlet will be modeled and propagated up to the connectivity boundary using some ray technique (such as the SBR [4]and the GRE [5] or modal method [6]) These techniques are well understood and this report is not concerned with their description and implementation. Instead, our emphasis is on the proposed techniques for modeling the complex cavity termination and coupling of the fields associated with the different techniques at the connectivity boundary. As noted earlier, the FEM will be used to model the fields in the vicinity of the complex cavity termination (i.e. to the right of the connection boundary). We could indeed use the modal or ray techniques to generate the excitation to the FEM system of equations. However, this approach would require the solution of the FEM system for each field excitation, a rather inefficient way of characterizing the interior cavity scattering at all incidence angles of the impinging plane wave. Instead, given that the cavity is circular at the connectivity boundary, a convenient way to characterize the termination is by determining its generalized modal scattering matrix. Since each field distribution at the connectivity boundary can be expressed as a sum of incoming (or outgoing) cylindrical waveguide modes, the modal scattering matrix provides us with a unique method for characterizing the cavity termination without consideration of the technique used for modeling the fields to the left or right of the connectivity boundary.

The generalized scattering matrix $[S]$ of a given termination relates the coefficients of the incoming modes to the coefficients of the corresponding outgoing modes. That is

$$[S]\,\{a\} = \{b\} \tag{1}$$

where the elements of the vectors $\{a\}$ and $\{b\}$ are simply the coefficients of the incoming and outgoing modes respectively. They are defined by

$$a_m = \frac{\int_\Gamma \bar{e}^{inc}(x, y, z_0) \cdot \bar{\Psi}^*{}_m(x, y, z_0)\, ds}{\int_\Gamma \bar{\Psi}_m(x, y, z_0) \cdot \bar{\Psi}^*{}_m(x, y, z_0)\, ds} \tag{2}$$

$$b_m = \frac{\int_\Gamma \bar{e}^{s}(x, y, z_0) \cdot \bar{\Psi}^{s*}{}_m(x, y, z_0)\, ds}{\int_\Gamma \bar{\Psi}^{s}_m(x, y, z_0) \cdot \bar{\Psi}^{s*}{}_m(x, y, z_0)\, ds} \tag{3}$$

for $m = 1, 2, 3, \ldots N$, in which $\bar{e}^{inc}$ and $\bar{e}^{s}$ are the incident and scattered transverse electric fields respectively, on the connectivity boundary surface Γ, and $\bar{\Psi}_m$ denotes the mode functions of the circular waveguide of a given radius. A single mode index is used to compactly represent the totality of

the even/odd, TE or TM modes, each of which is associated with indices n and p. The explicit form of $\overline{\Psi}_m$ is given in the appendix.

In accordance with the proposed FEM-modal method, the entries of the generalized scattering matrix are computed from the solution of the FEM system. More specifically, the FEM solution proceeds as follows:

Given that the cavity accomodates N traveling modes

(a) Use the q'th mode as the excitation

(b) Find a_q at the connectivity boundary Γ

(c) Solve the finite element system to find the scattered field

(d) Calculate the innerproduct of the scattered field with each out-going traveling mode on the connectivity boundary Γ to find b_p $(p = 1, 2, 3, \ldots N)$

(e) Calculate the q'th column of the scattering matrix as $S_{pq} = \frac{b_p}{a_q}$

(f) Repeat for all $q = 1, 2, 3, \ldots N$

We remark that if the connectivity boundary is placed a distance $\frac{1}{4}\lambda$ from the cavity termination, only propagating modes need be considered without compromising accuracy.

We note that the generalized scattering matrix has certain distinct properties:

- Its size is N x N, where N is the number of traveling modes (See Table 1).
- It is symmetric and unitary since all modes are defined to have the same power.
- It has so far been observed to be sparse since the incoming modes tend to couple more strongly to those outgoing modes having indices in the proximity of the incoming mode. As an example, we illustrate in Figure 2 the scattering matrix for a stub terminated inlet. The shown results were generated via the theoretically exact mode-matching technique [7]. Note that the single index m used for ordering the modes in Figure 2 is given in Table 3.

Given the generalized scattering matrix of the termination, the evaluation of the scattered field from the structure is feasible. Since the incident field is known, the coefficients $\{a\}$ of the incoming modes are also known [10], therefore the coefficients $\{b\}$ of the outgoing modes can be readily evaluated by (1). In the context of the modal technique, all outgoing modes are tracked to the open end, where an aperture integration is performed to calculate the radiated field. Since Aperture Integration is based on the Physical Optics approximation, it is often necessary to correct the result by including the effect of the rim, i.e. by considering the contribution of the Ufimtsev currents [9]. The total far field can be evaluated in closed form for rectangular or cylindrical inlet cross-sections [10]. Note that there is some reflection of the outgoing modes from the open mouth back to the inlet, but this effect is usually negligeable.

If the inlet is electrically very wide, one can employ high frequency techniques to model the propagation through the inlet body. The most commonly used techniques are the Shooting and Bouncing Ray method (SBR) [4], and the Generalized Ray Expansion (GRE) [5]. Neither of them is as accurate as the exact modal method, but they are much simpler from a computational point of view. Moreover, unlike the modal technique, they do not require that the geometry be of canonical shape.

In the context of the SBR method, the incident field on the open end is decomposed into a set of parallel ray tubes which are tracked into the cavity. When using the GRE method, the open end aperture is divided into a number of subapartures, and the incident field is decomposed into a set of rays emanating from each subaperture. Unlike the SBR, the rays are not necessarily parallel to each other, and GRE is thus capable of tracing non-planar wavefronts. Regardlesss of which method is used (SBR or GRE), as soon as the rays reach the connectivity boundary, the incoming field is transformed into a superposition of modes using (2) (it is assumed that modes can be defined in the vicinity of the connectivity boundary). The generalized scattering matrix is then computed via the FEM analysis and the amplitudes of the out-going modes are computed from (1). The scattered field can be evaluated by means of the Reciprocity Integral method [11] thus elliminating the need to track the rays back to the open end.

3.0 Finite Element Analysis

The traditional FEM analysis involves the solution of the time harmonic, weak form of the wave equation in a bounded volumetric region of space. Being a partial differential equation method, the FEM analysis leads to sparse matrices (with about 10 to 50 nonzero entries per row) and permits the modeling of complex inhomogeneous regions without a need for special care and considerations. For our problem at hand, the FEM analysis region is shown in Figure 3 and is seen to extend a bit beyond the connectivity boundary Γ to a mesh termination boundary Γ'. On Γ' it is necessary to enforce an absorbing boundary condition (ABC) or some other mesh termination scheme which ensures the outgoing nature of the waves. That is, Γ' must be a non-reflecting boundary and this will be discussed later in more detail. We remark that the cross section between Γ and Γ' is again assumed circular for this analysis but this assumption has no bearing on the actual cavity of Figure 1.

On the basis of the FEM-modal formulation, we are interested in computing the fields scattered by the cavity termination due to the modal excitation

$$\bar{E}^{inc} = \bar{\Psi}_q \tag{4}$$

The total field in the FEM region is then given by

$$\bar{E} = \bar{E}^{inc} + \bar{E}^s \tag{5}$$

and it is well known that the unknown scattered electric field satisfies the weak wave equation (see for example [1],[2] and [13])

$$\begin{aligned} &\int_{\Gamma'}\int \left(\frac{1}{\mu_r}\bar{T}\cdot\left[\hat{n}\times(\nabla\times\bar{E}^s)\right]\right)ds + \int_{\Omega}\int\int\left(\frac{1}{\mu_r}(\nabla\times\bar{E}^s)\,(\nabla\times\bar{T}) - k_0^2\varepsilon_r\bar{T}\cdot\bar{E}^s\right)dv = \\ &-\int_{\Gamma'}\int \left(\frac{1}{\mu_r}\bar{T}\cdot\left[\hat{n}\times(\nabla\times\bar{E}^{inc})\right]\right)ds - \int_{\Omega}\int\int\left(\frac{1}{\mu_r}(\nabla\times\bar{E}^{inc})\,(\nabla\times\bar{T}) - k_0^2\varepsilon_r\bar{T}\cdot\bar{E}^{inc}\right)dv \end{aligned} \tag{6}$$

where $\bar{T}$ is referred to as a testing function and must be at least square integrable. For Galerkin implementations, $\bar{T}$ is set equal to one of the expansion basis and for each basis, a system equation is constructed. However, before proceeding with the system construction, it is necessary to first introduce the magnetic field $\bar{H}^s = \dfrac{\nabla\times\bar{E}^s}{j\omega\mu_0\mu_r}$ and rewrite the above weak equation as

$$\iiint_{\Omega}\left\{\frac{1}{\mu_r}(\nabla\times\bar{E}^s\cdot\nabla\times\bar{T})-\bar{T}\cdot k_0^2\varepsilon_r\bar{E}^s\right\}dv-\iint_{\Gamma'}\{jk_0\eta\bar{T}\cdot(\hat{n}\times\bar{H}^s)\}\,ds+$$

$$\iiint_{\Omega}\left\{\frac{1}{\mu_r}(\nabla\cdot\bar{E}^s)(\nabla\cdot\bar{T})\right\}dv= \tag{7}$$

$$-\iint_{\Gamma_d}\left\{\left[\frac{1}{\mu_{r2}}-\frac{1}{\mu_{r1}}\right]\bar{T}\cdot(\hat{n}_d\times(\nabla\times\bar{E}^{inc}))\right\}ds-\iint_{\Gamma'}\left\{\frac{1}{\mu_r}\bar{T}\cdot(\hat{n}\times(\nabla\times\bar{E}^{inc}))\right\}ds$$

in which Γ_d represents the surface over dielectric boundary discontinuities between regions of different magnetic permeability. Note that $\hat{n}_d$ points from μ_{r2} to μ_{r1} and only material discontinuities within the scatterer, not the fictitious absorber contribute to the boundary integral on Γ_d. Also, the third term on the left hand side of (7) is the usual penalty term which ensures that the divergence condition be satisfied in the Galerkin least squares sense. This will be discussed later in more detail.

On our way to discretizing the weighted residual equation given above, it is necessary to: (a) tessellate the volume Ω into smaller elements, (b) choose an expansion for the field in each element and (c) to relate $\bar{H}^s$ and $\bar{E}^s$ on the outer boundary of Ω including Γ'. These issues are addressed in the next section.

4.0 Implementation of the FEM Solution

Creating user-oriented and efficient software to implement the above FEM formulation requires that a number of issues be addressed. First, the most appropriate shape and elements must be chosen. Also, since the problems will be large, efficient pre-processing software must be created to extract (from a given mesh) information needed to enforce the boundary conditions. This includes finding metal surfaces and edges, corners, normals, material discontinuities and the elements on the connectivity boundary. It is also crucial to develop preprocessing algorithms that run in O(n) time for a general mesh. To this end, an efficient preprocessor has been created for extracting relevant information from an arbitrary three-dimensional tetrahedral mesh [12]. The issues related to elements and field expansion will be examined now as they pertain to the inlet problem.

4.1 Elements and Field Expansions

There are two classes of field expansions that could be used with tetrahedral elements: node based and edge based expansions. Edge-based elements are a better choice than node-based elements for the eigenvalue problem because standard node-based elements cannot accurately represent the eigenvectors (fields) that correspond to zero eigenvalues. All of the eigenvalues that should be zero (one for each internal degree of freedom) have some small non-zero value when using standard node-based elements. This large scale degeneracy causes considerable numerical problems when computating the eigenvalues especially for large systems. When using edge-based elements, the eigenvalues are cleanly split into zero and non-zero groups thus alleviating much of the numerical problems [15]. (That is, the zero eigenvalues are identically zero.)

The 'penalty' term has been used with node based elements to shift the resonant frequencies of the eigenvalues that should be zero, up above the sample rate of the mesh [16]. Unfortunately, this 'penalty' term also shifts correct eigenvalues to an unpredictable degree. During the course of this study a number of other schemes were examined with the goal of improving the accuracy of node based elements for eigenvalue computations. One method was to use a numerical bi-linear shape function that couples an internal degree of freedom to all other degrees of freedom by enforcing the divergence condition exactly. This was found to work well on small problems but became unwieldy to apply on larger problems. Another technique was to use a purely imaginary penalty term (multiplying the penalty term in (2) by j) which tended to shift only the imaginary parts of the eigenvalues, leaving the real parts close to their correct values. The real dominant eigenvalues were those whose imaginary parts were the smallest and could therefore be separated from the spurious eigenvalues whose imaginary parts were relatively large.

Although edge-based elements are indeed better for eigenvalue problems, the best choice of elements for three-dimensional scattering analysis is not clear. Both classes of elements were considered (node-based and edge-based) for this problem.

Node-based elements

When using linear node based elements, the scattered field is given by

$$\bar{E}^s = \sum_{a=1}^{4} (\hat{x} N_x^a E_x^a + \hat{y} N_y^a E_y^a + \hat{z} N_z^a E_z^a)$$

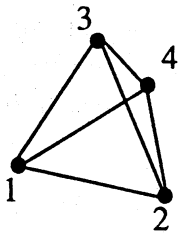

where

$$N_x^a = N_y^a = N_z^a = N^a(x, y, z)$$

are the standard scalar shape functions [1] and E_x^a, E_y^a and E_z^a are the components of the vector degrees of freedom associated with each of the four nodes.

By numerical experimentation was found that boundary conditions for these elements must be implemented carefully to avoid deterioration the system condition. For a node lying on a conductor, two tangent vectors can be defined from the surface normal, such that

$$\begin{aligned} \hat{t}_1 \cdot \bar{E}^s &= -\hat{t}_1 \cdot \bar{E}^{inc} \\ \hat{t}_2 \cdot \bar{E}^s &= -\hat{t}_2 \cdot \bar{E}^{inc} \end{aligned} \tag{8}$$

where $\hat{t}_{1,2}$ denote the rthonormal unit vectors tangent to the metallic surface. There are many possible ways of coupling the global equations to enforce the boundary conditions (8), but there is always a best way which preserves the system's condition. If the boundary conditions are enforced arbitrarily, it is possible to completely destroy the condition of the system and to generate wrong results. The following procedure will guarantee a well conditioned final system:

Given the metal surface normal $\hat{n}$ at the node, find the two tangent vectors $\hat{t}_1$ and $\hat{t}_2$ as follows

- if $|\hat{y} \times \hat{n}| > 0.15$ then set $\hat{t}_1 = \dfrac{\hat{y} \times \hat{n}}{|\hat{y} \times \hat{n}|}$

  else set $\hat{t}_1 = \dfrac{\hat{x} \times \hat{n}}{|\hat{x} \times \hat{n}|}$

- $\hat{t}_2 = \dfrac{\hat{t}_1 \times \hat{n}}{|\hat{t}_1 \times \hat{n}|}$

- Given the three global equations for E_x^a, E_y^a and E_z^a at the node

  - find the largest component of $\hat{t}_1$ (x, y or z) and replace the corresponding global equation with $\hat{t}_1 \cdot \bar{E}^s = -\hat{t}_1 \cdot \bar{E}^{inc}$

  - find the largest component of $\hat{t}_2$ (x, y or z) and replace the corresponding global equation with $\hat{t}_2 \cdot \bar{E}^s = -\hat{t}_2 \cdot \bar{E}^{inc}$

Tangential continuity of the electric field across material discontinuities is enforced automatically during assembly of the system without a need for double noding. However, it is also necessary to enforce continuity of the normal electric flux vector ($\bar{D}$) across interfaces where the electric permittivity changes. This can be done using a technique given in [13] where one degree of freedom on one side of the interface is written in terms of the degree of freedom on the other side by enforcing

$$\varepsilon_1 \hat{n} \cdot \bar{E}_1 = \varepsilon_2 \hat{n} \cdot \bar{E}_2$$

across the interface from region 1 to region 2.

Edge-based elements

The first order, vector, edge based, tetrahedral elements given in [14]expand the unknown field as

$$\bar{E}^s = \sum_{a=1}^{6} \bar{N}_a E_a$$

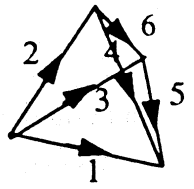

where $\bar{N}_a$ is the vector shape function associated with the a'th edge. The scalar degrees of freedom E_a refer to the component of the scattered field directed along the a'th edge.

These elements were implemented for the inlet termination scattering problem and were found to break down when the scattered field was purely TE (no z component of the scattered electric field). This breakdown is highly mesh dependant and is manifested in a poorly conditioned global system. Clearly, if a vector field at the center of a given edge of an element is orthogonal to that edge, edge-based elements cannot represent that field and yield a singular system. When a large volume is filled with a free tetrahedral mesh and the solution is purely TE, apparently a nearly singular system may result.

Since it is the job of the FEM to find the modal coupling, and since this coupling may in some cases be pure TE, the elements must be able to accurately represent a pure TE field while at the same time represent other types of fields. Because of the above difficulties for edge-based elements in modeling pure TE fields,we resorted to the node-based elemenst for this application.

4.2 Mesh Termination Schemes

At the open end of the mesh, the fields radiate into an infinite, cylindrical waveguide. The boundary condition at this open end must absorb all traveling modes in the guide (see Figure 3). The most obvious choice is to expand the scattered field as a sum of all traveling modes and couple this expansion directly to the FEM equations.

Let the tangential electric field at the open end be given by

$$\bar{e}^s = \sum_{m=1}^{M} b_m \bar{\Psi}_m^s \tag{9}$$

where b_m ar unknown coefficients and $\bar{\Psi}_m^s$ is given in (3). Substitution of this expansion into the second term of (7) yields

$$\iint_\Gamma \{jk_0\eta \bar{T} \cdot (\hat{n} \times \bar{H}^s)\}\, ds \rightarrow \iint_\Gamma \{\frac{1}{\mu_r}\bar{T} \cdot \left(\sum_{m=1}^{M} b_m \hat{n} \times (\nabla \times \bar{\Psi}_m^s)\right)\}\, ds \tag{10}$$

With the introduction of the new coefficients b_m, to solve the system, resulting form (7), it is necessary to construct additional equations. These are given by

$$b_m = \frac{\int_{\Gamma} \bar{e}^s(x, y, z_0) \cdot \bar{\Psi}^{s^*}{}_m(x, y, z_0)\, ds}{\int_{\Gamma} \bar{\Psi}^s_m(x, y, z_0) \cdot \bar{\Psi}^{s^*}{}_m(x, y, z_0)\, ds} \tag{11}$$

and couple each unknown coefficien b_m to the fields associated with nodes on Γ'. This leads to a sparse, square (FEM) system coupled to a dense, rectangular (modal expansion) system.

While this scheme worked for shorted inlets, it was found to be unstable for the stub terminated inlet. Even if it were not for this instability, the full submatrix resulting from this scheme would make it impractical for large radius cavities. A more efficient scheme is to use a fictitious material absorber designed especially for cylindrical, traveling modes. The use of material absorbers in FEM computation also preserves the sparsity of the overall system and results in a better conditioned system than other mesh termination schemes such as numerical absorbing boundary conditions

The design of a fictitious material absorber to absorb all traveling modes is complicated because the impedance and propagation constants of these modes vary greatly. The impedance of the first eight traveling modes for a guide of radius 0.66λ is given in Table 2. These eight modes were used to design an optimized absorber. Clearly, if the absorber were allowed to be very long, a nearly perfect absorber could be constructed. However, since the absorber will be part of the FEM mesh, as a design constraint, it should be no more than about a half of a free space wavelength long to be practical.

A Monte Carlo optimization scheme [17] was used that has the desirable property of finding not only the best performing but also the most stable design. A five section, metal backed absorber was used as a starting point with ε_r and μ_r set to unity in each section. The length of each section was set initially to $.1\lambda$. The 15 parameters (material constants and lengths of each section) were varied randomly, independent of one another. Transmission line theory was used to calculate the reflection coefficient for each mode (see Figure 4), and the algebraic sum of reflection coefficients (the sum of absolute values) was used as the global optimization parameter. A pass/fail criterion on the global parameter was set to give about a 50% yield. For each random design, a pass or fail was noted for each parameter and after a number of designs have been sampled, a pattern begins to emerge. Some parameters indicate a tightening up is in order since most of the 'good' designs were centered about a certain value. Other parameters indicate a don't care condition as all values worked equally well. A new set of initial values and ranges is chosen and the process is restarted. Again, the global parameter threshold is choosen to give about a 50% yield. This global threshold continues to drop each iteration until a stable design is found.

The final design and its performance is shown in Figure 5. Note that the reflection coefficient for all modes is less than .1 (-10 dB). The performance of this absorber was tested for a larger guide of radius 2λ having 77 traveling modes and from Figure 6 it is seen to have good broad band performance.

There are many advantages to using the optimized fictitious absorber for terminating the mesh. First, the condition of the FEM system is actually improved through the use of this type of truncation scheme. While a local or global ABC would require a smaller mesh, this savings becomes less important as the problem size increases since the absorber will take up a smaller fraction of the total volume.

5.0 Examples

Example 1

The simplest configuration that could be analyzed is a cylindrical cavity terminated with a flat plate. To terminate the FEM mesh the absorber was placed 0.33λ away from the cavity base. We remark that no mode coupling is present in this configuration and that the mesh was generated using SDRC I-DEAS with a global element size of $\frac{1}{12}\lambda$. For this calculation, the connectivity boundary was placed 0.15λ from the base and the scattering matrix calculated using the FEM-modal formulation was used to calculate the outgoing mode coefficients. These modes were then traced back out of the inlet to find the radiated field. The results are shown in Figure 7 for a 1λ long and 1.32λ wide cylindrical cavity. Good agreement is seen as compared to a mode matching solution [7].

Example 2

The next simplest cavity termination is a circular stub. This geometry also can be analyzed via a mode matching solution [3] since all of the conductors are on curves of constant coordinates. The absorber was placed 0.33λ from the stub and the scattering matrix was computed at a distance of 0.25λ in front of the stub. Figure 8 shows a cut of the volume mesh for this configuration and the co-polarized backscatter patterns are given in Figure 9.

It was found that the proper handling of the boundary conditions at the inner edge (the rim of the stub) was critical. If the total field were set to zero at this inner edge, the results were quite wrong. However, if only the component tangential to the edge (E_ϕ) was set to zero, whereas E_z was allowed to float, the results were much improved and this is shown in Figure 9.

While the shown results are in good agreement for horizontal polarization, there is some discrepancy in the vertical polarization. Finer sampling around the rim does improve the comparison slightly but with very slow convergence. The result shown were obtained using a global element size of $\frac{1}{12}\lambda$ and an element size of $\frac{1}{20}\lambda$ around the rim.

6.0 Conclusions

The benchmark tests show the validity of the overall FEM-modal scheme and the utility of the broadband cylindrical mode absorber for terminating the mesh. Also, the results indicate that node-based elements can be used for scattering analysis if boundary conditions are handled properly so as not to disturb the condition of the FEM system. Since the edge elements broke down for the pure TE case, no comparison between edge and node-based elements was possible for this problem. For example, the TE_{21e} mode couples only to itself for the circular stub, giving rise to a pure TE field in the front portion of the mesh.

There were many different methods and schemes tried before the above formulation was settled on. A mode matching technique for terminating the mesh was tried but was found to be unstable and to lead to large storage requirements. A mathematical absorbing boundary condition was considered, but have been found to produce poorly conditioned systems in comparison to fictitious material absorbers. Thus, we resorted to a material absorber for terminating the mesh and this was shown to have good modal absorption for inlets larger than was initially considered. Apparently, the first set of traveling modes cover such a wide range of impedances and propagation constants that the higher order modes are also absorbed.

While the good results obtained for the stub (for horizontal polarization) show that the overall method is promising for irregular terminations, the errors seen for vertical polarization indicate that more work needs to be done in the fundamental aspects of the finite element method for electromagnetic scattering problems especially in the area of special elements, or new techniques to accurately model fields that are very slowly converging.

7.0 Future Work

The next set of benchmarks will consist of bodies of revolution (BOR) as these geometries possess reference solutions from available BOR moment method codes. Also, a ridge termination will be analyzed as this possesses a mode matching solution. If the ridges are curved, a simple model of a fan is created. This configuration may possess a mode matching solution.

Eventually, realistic engine geometries will be explored. Here the greatest challenge will be the computational intensity. An inlet with a radius of 50 wavelengths and a depth of 3 wavelengths could easily have over 100 million degrees of freedom making a brute force solution impossible.

The following two types of symmetry can be exploited to make the problem more manageable.

- Geometric symmetry

  Only one 'pie' slice of the geometry need be meshed since the fan blades have periodic angular symmetry. Other elements are simply an angular offset from the 'pie' slice.

- Modal symmetry

  The modes themselves are symmetric about some annulus since they have a $\sin(n\phi)$ or $\cos(n\phi)$ angular dependance.

The sparse finite element system can therefore be considered to be a sum of sparse systems.

$$[[K_1] + [K_2] + [K_3] \ldots] \{\{\phi_1\} + \{\phi_2\} + \{\phi_3\} \ldots\} = \{\{f_1\} + \{f_2\} + \{f_3\} \ldots\}$$

where $[K_1]$ is the finite element system for the 'pie' slice and the other systems are the same except that their entries point to an offset group of degrees of freedom, overlapping at the interfaces of the regions. This scheme requires that the mesh be generated with coincident nodes and elements on the two inner sides of the pie slice, a property that cannot be guaranteed by commercially available mesh generators. Exploiting the geometric symmetry would require considerable work with the mesh generation software.

It is possible however to define local nodes on one face that coincide with the nodes on the other face by interpolating between the existing nodes. In this way, no modifications would need to be done to the mesh but there will be an increase in the number of degrees of freedom. Also, this may lead to numerical instabilities as the condition of the system is highly dependant on the location of these new, interpolated degrees of freedom.

An important special case however, is if the geometry internal to the pie slice has symmetry within itself. Considering that the mesh will consist primarily of overlapping fan blades, there will be odd symmetry about a midline in the pie slice. This will make it easy to guarantee coincident nodes and elements on the two sides of the slice.

If this geometric symmetry can indeed be exploited so that only one 'pie' slice of the system need be stored, then a new matrix-vector product routine will need to be created to handle this operation.

This routine will be made to run efficiently in parallel on one of the available parallel machines such as the KSR or Intel Paragon.

The symmetry of the modal fields is less important as savings in memory would be much less as compared to the savings due to the geometric symmetry. It is also unclear how to proceed since the scattered field in general will contain many modes, all with different angular symmetry. It is only when the modal symmetry and the geometric symmetry are coincident that the net scattered field will posses angular symmetry that can be exploited.

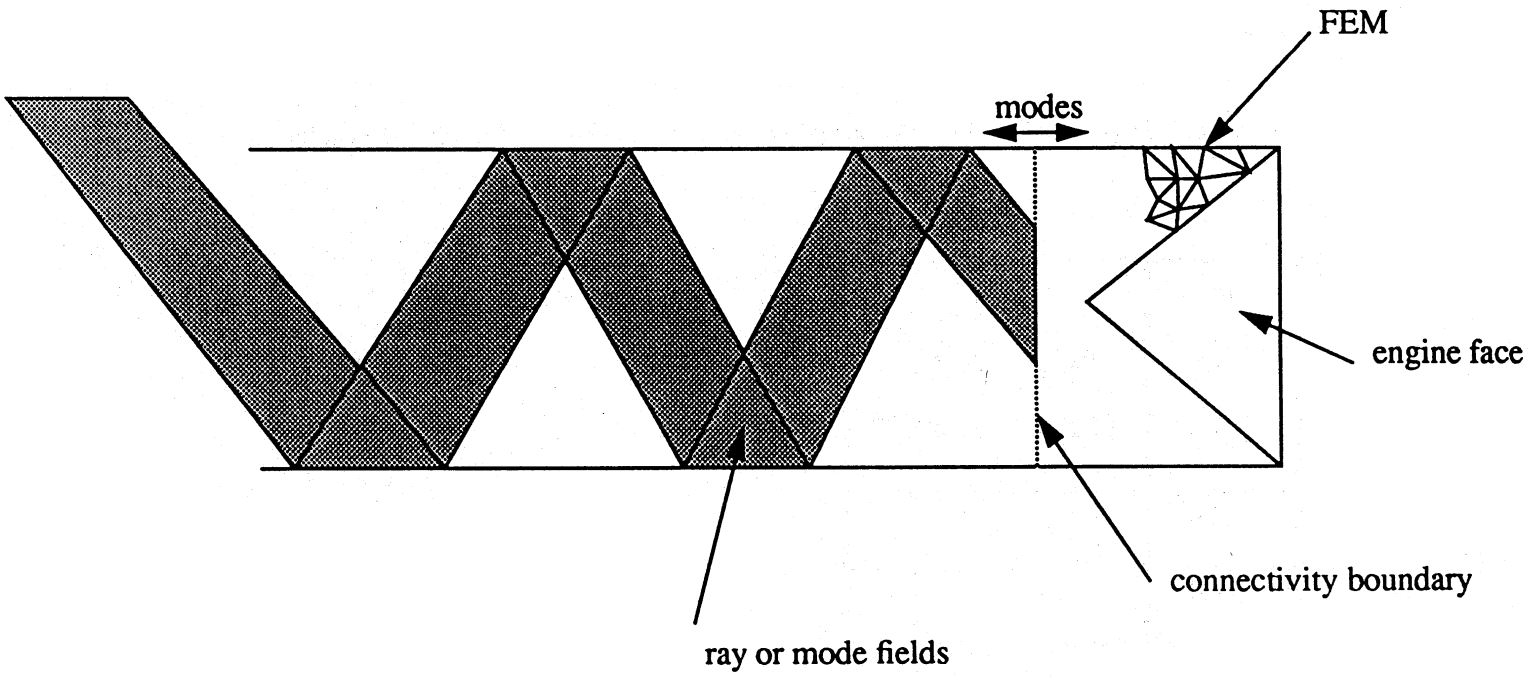

FIGURE 1. Hybrid jet engine inlet analysis.

radius (λ)	.5	.66	1.66	3	4	5	10
N	6	10	60	186	328	508	2008

TABLE 1. Number of traveling modes for different radii cylindrical guides.

Mode	TM^e_{01}	TM^e_{11}	TE^o_{11}	TE^o_{21}	TM^o_{11}	TE^e_{01}	TE^e_{11}	TE^e
Z (Ω)	307	144	421	557	144	986	421	557

TABLE 2. Impedance of the eight traveling modes in a cylindrical guide with radius 0.66λ.

m	Mode
1-10	$TM^e_{0,1}$ - $TM^e_{0,10}$
11-20	$TM^e_{1,1}$ - $TM^e_{1,10}$
21-30	$TM^e_{2,1}$ - $TM^e_{2,10}$
31-40	$TE^o_{0,1}$ - $TE^o_{0,10}$
41-50	$TE^o_{1,1}$ - $TE^o_{1,10}$
51-60	$TE^o_{2,1}$ - $TE^o_{2,10}$

TABLE 3. Mode indices corresponding to the results in Figure 2

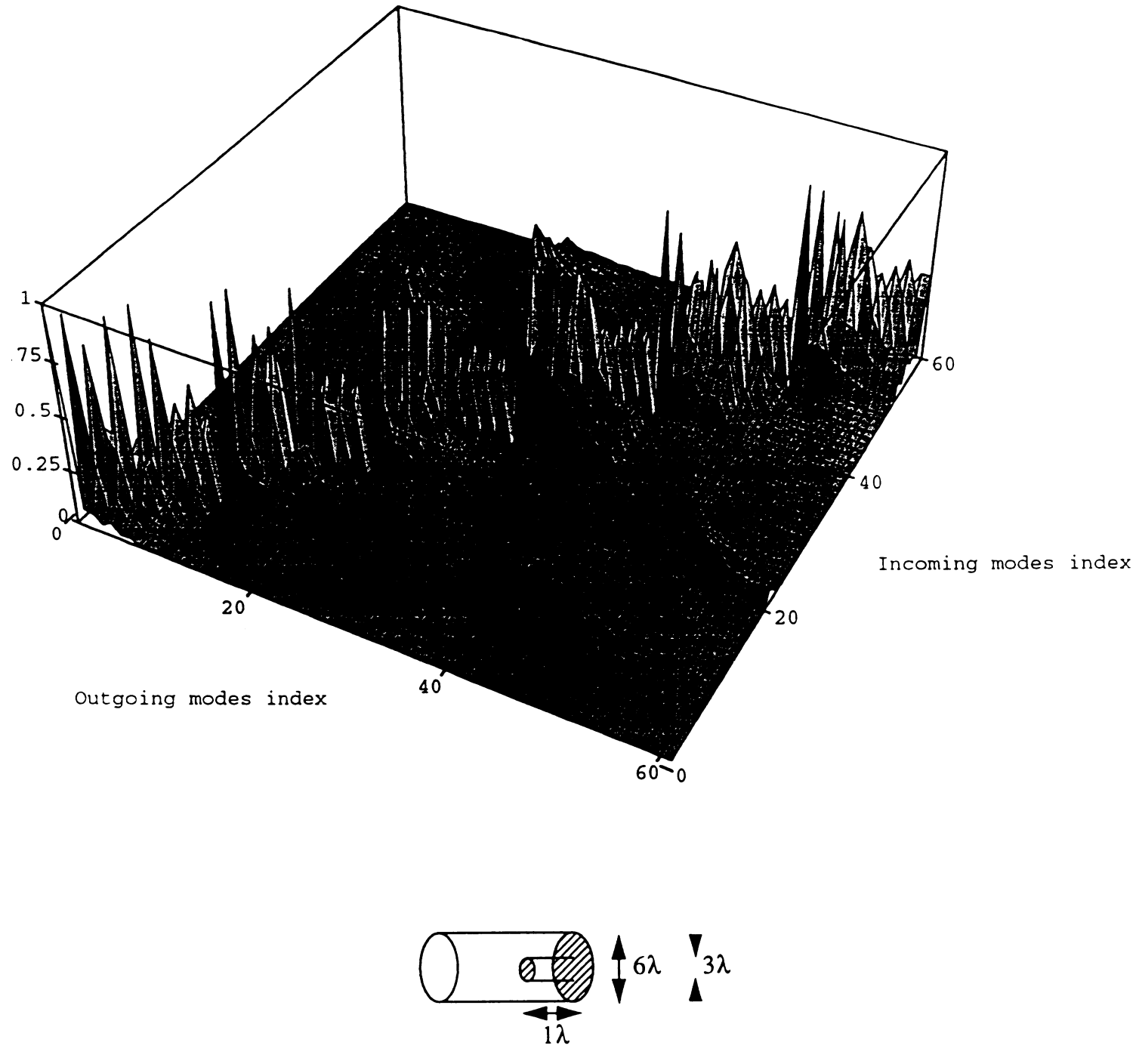

FIGURE 2. Amplitudes of the elements of the generalized scattering matrix calculated by mode-matching for a hub termination.

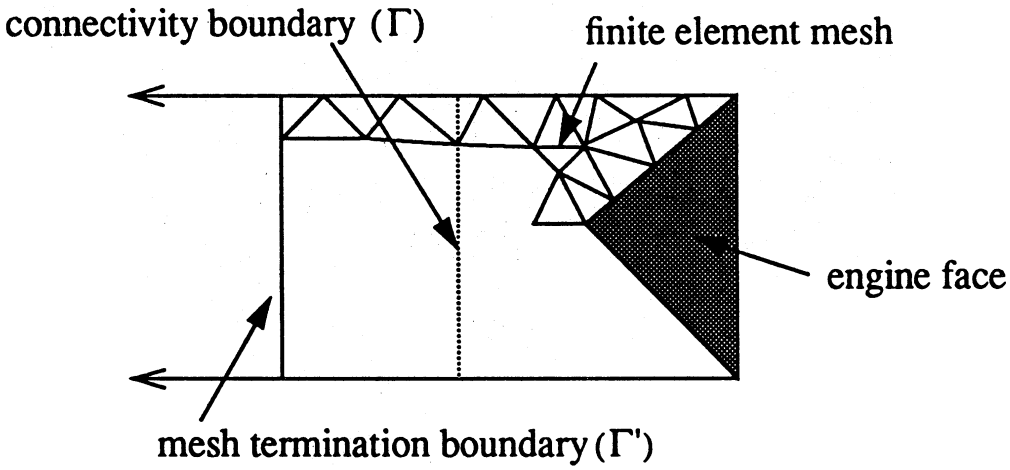

FIGURE 3. Engine face region where finite element analysis is applied

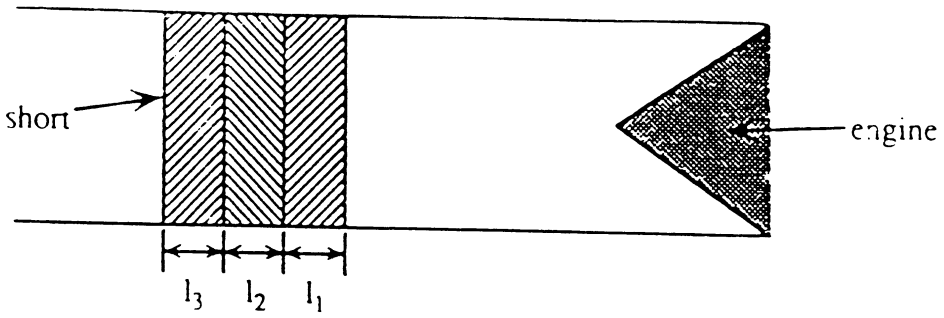

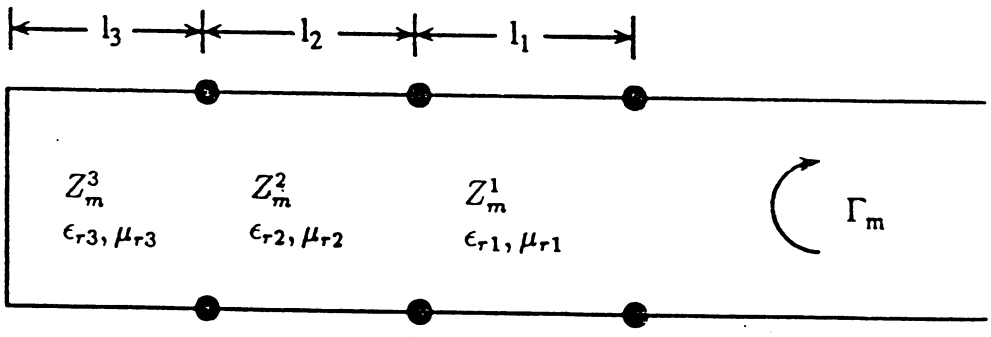

$$Z_m^{i\mathrm{TE}} = \frac{Z_i k_i}{k_{z_i}} \qquad Z_m^{i\mathrm{TM}} = \frac{Z_i k_{z_i}}{k_i}$$

$$Z_i = Z_0 \sqrt{\frac{\mu_{ri}}{\epsilon_{ri}}} \qquad k_i = k_0 \sqrt{\epsilon_{ri}\mu_{ri}}$$

FIGURE 4. Transmission line model of cylindrical waveguide absorber

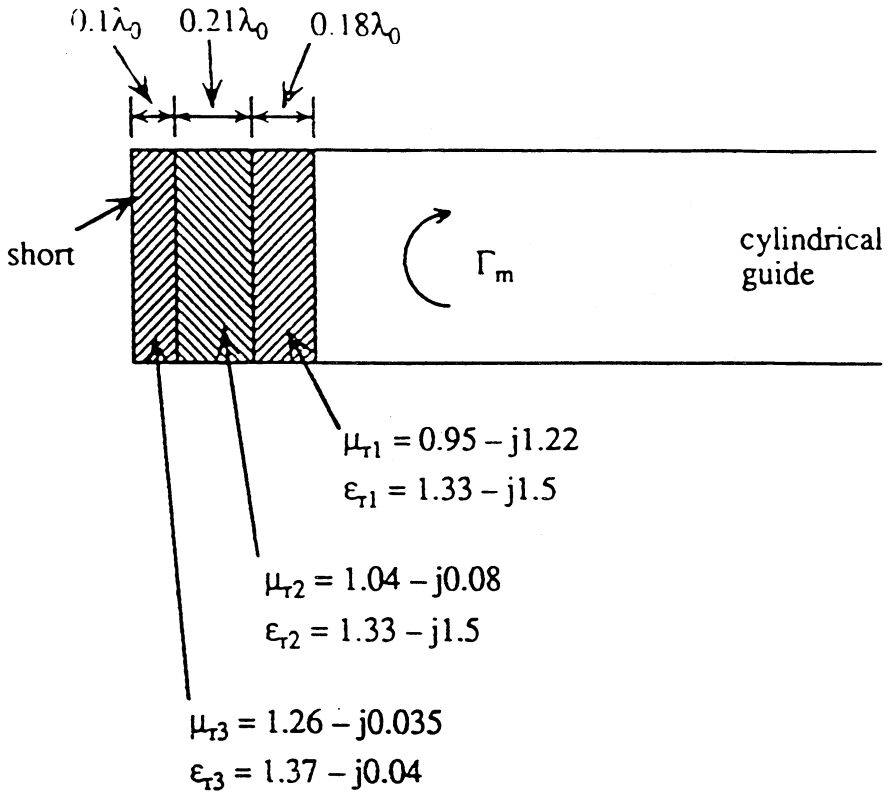

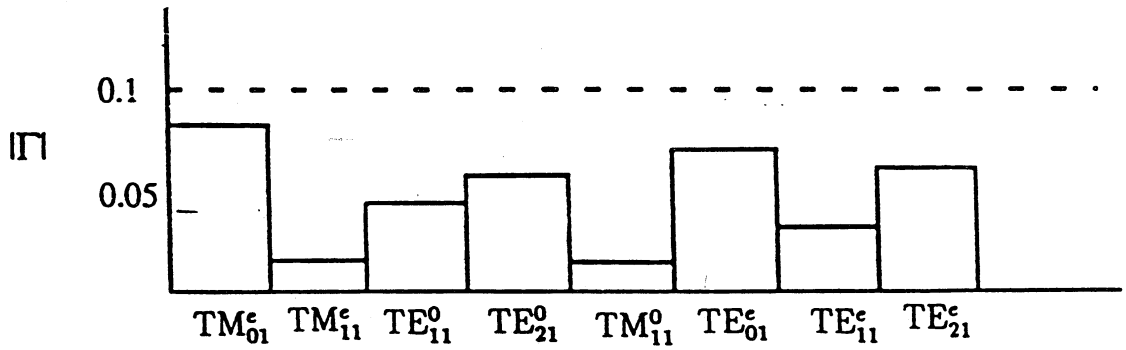

Modal reflection coefficients from absorber
($|\Gamma_m| < 0.1$ for all modes)

FIGURE 5. Optimum cylindrical waveguide absorber.

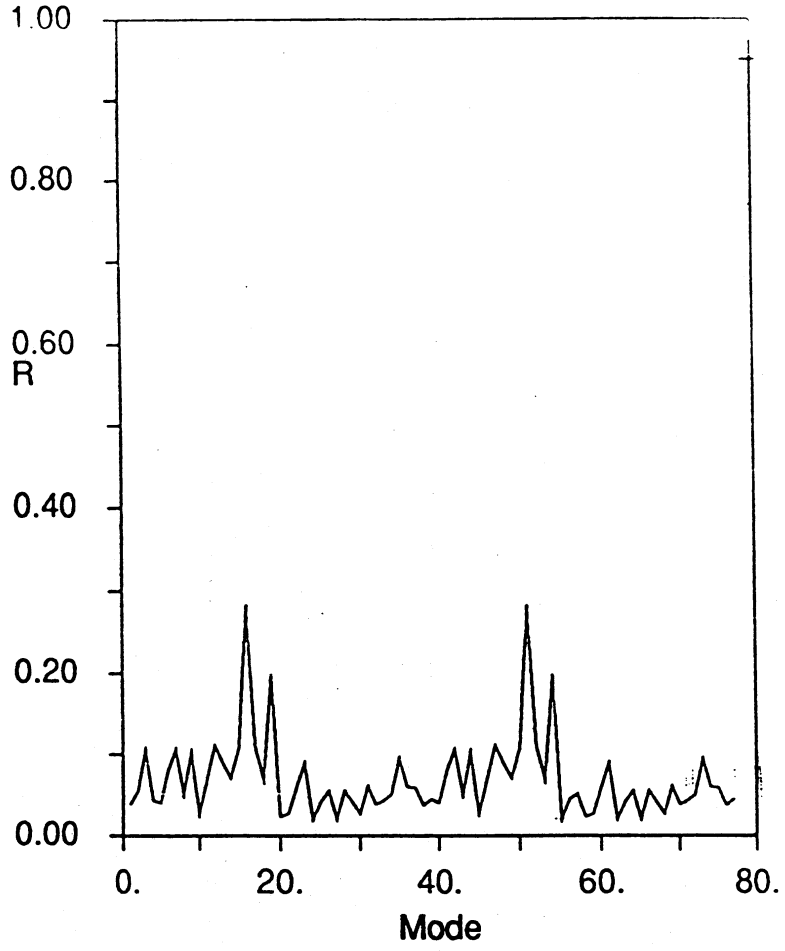

FIGURE 6. Performance of optimum absorber for the 77 travelling modes in a guide of radius 2λ.

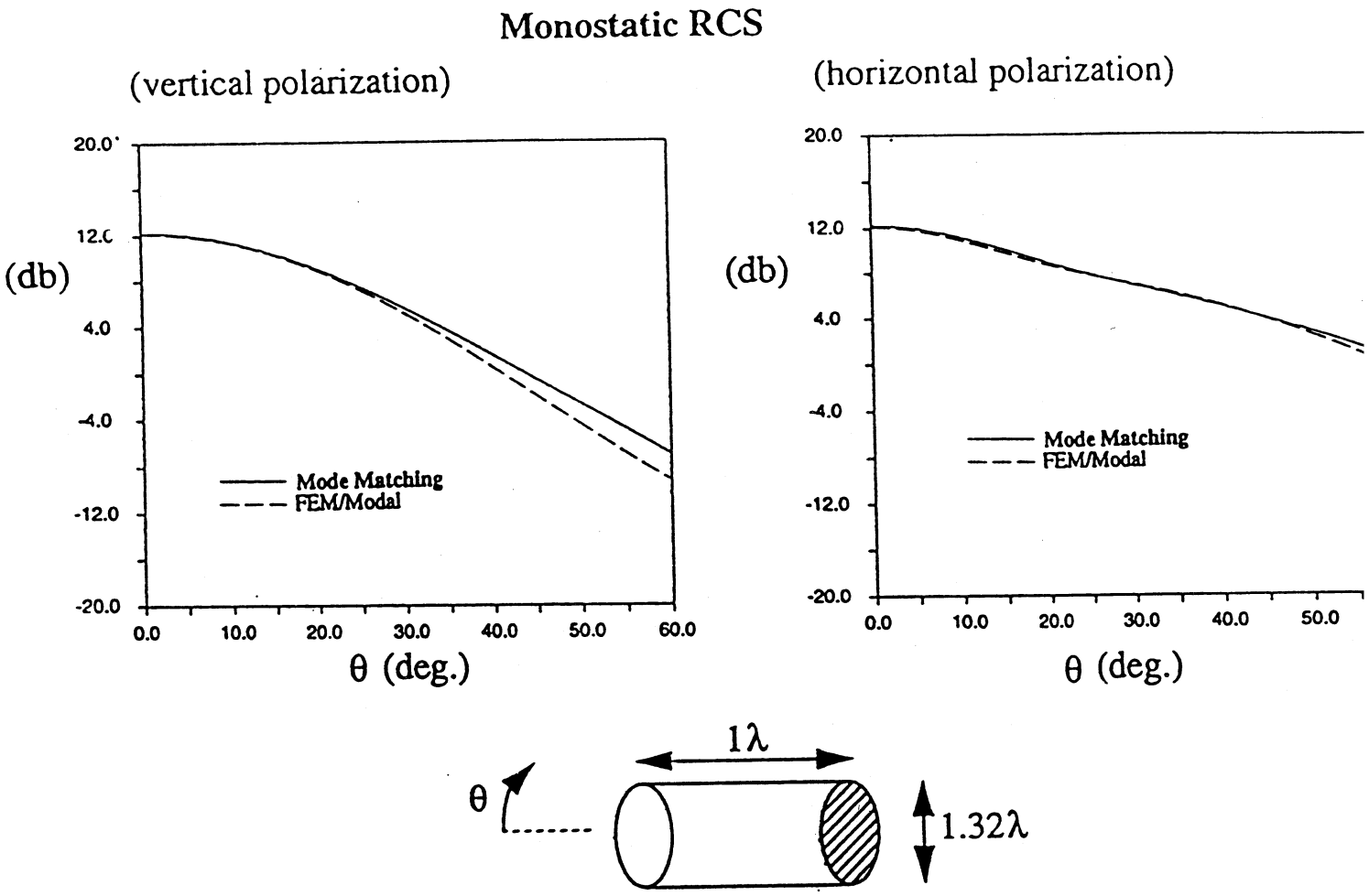

FIGURE 7. Results for example 1: a shorted cylindrical cavity

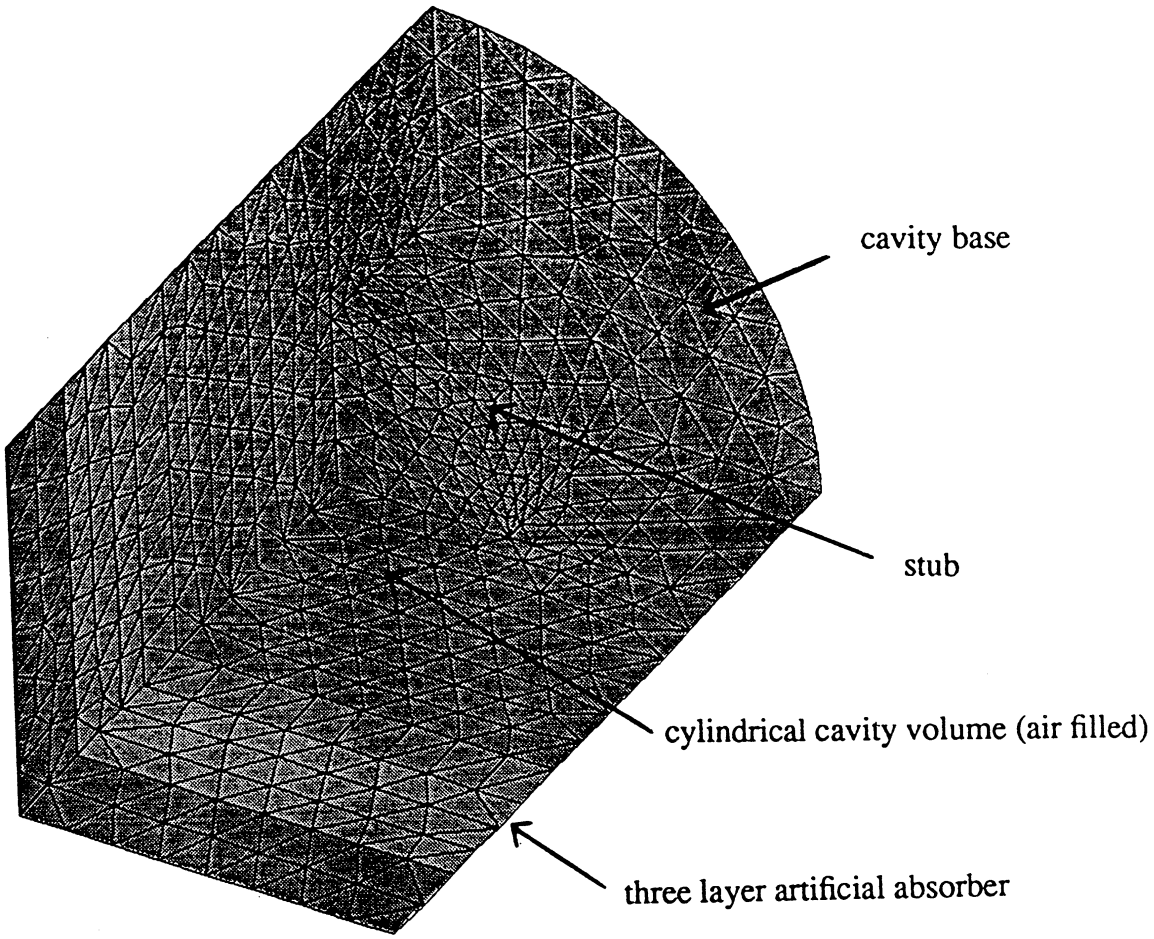

FIGURE 8. Illustration of the volume mesh for a stub terminated cylindrical cavity (1/4 of the geometry is shown)

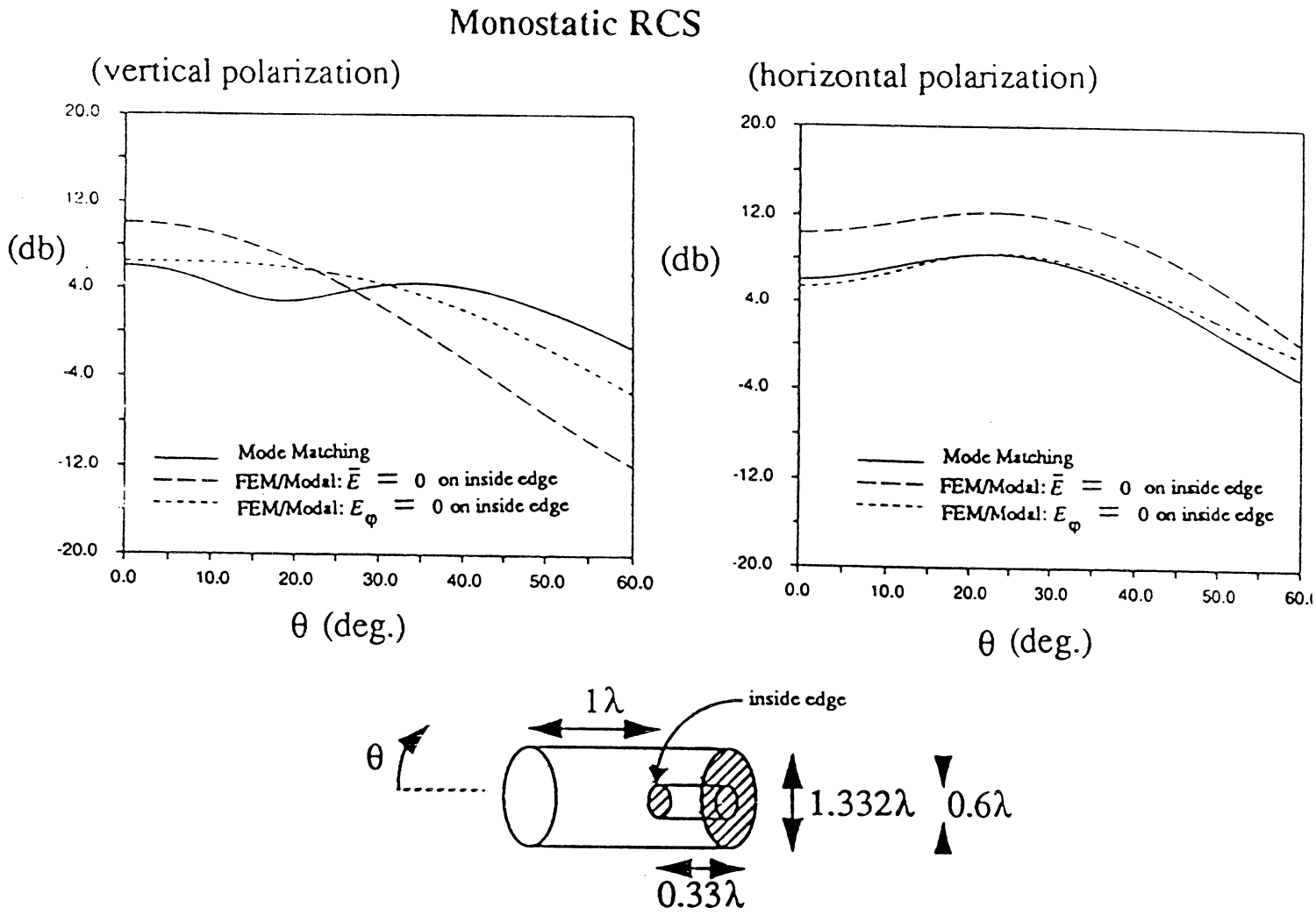

FIGURE 9. Results for example 2. A stub terminated inlet.

Appendix

The cylindrical mode functions $\overline{\Psi}_m$ are given by

$$\overline{\Psi}_m = \hat{\rho}E_\rho + \hat{\phi}E_\phi + \hat{z}E_z \tag{1}$$

where

$$E_\rho = e^{jk_z z}\begin{cases} N_{np}^{TE}\frac{n}{\rho}J_n(\frac{x'_{np}}{a}\rho)\sin n\phi & TE_{np}^e \\ -N_{np}^{TE}\frac{n}{\rho}J_n(\frac{x'_{np}}{a}\rho)\cos n\phi & TE_{np}^o \\ N_{np}^{TM}k_z\frac{x_{np}}{a}J'_n(\frac{x_{np}}{a}\rho)\cos n\phi & TM_{np}^e \\ N_{np}^{TM}k_z\frac{x_{np}}{a}J'_n(\frac{x_{np}}{a}\rho)\sin n\phi & TM_{np}^o \end{cases}$$

$$E_\phi = e^{jk_z z}\begin{cases} N_{np}^{TE}\frac{x'_{np}}{a}J'_n(\frac{x'_{np}}{a}\rho)\cos n\phi & TE_{np}^e \\ N_{np}^{TE}\frac{x'_{np}}{a}J'_n(\frac{x'_{np}}{a}\rho)\sin n\phi & TE_{np}^o \\ -N_{np}^{TM}\frac{nk_z}{\rho}J_n(\frac{x_{np}}{a}\rho)\sin n\phi & TM_{np}^e \\ N^{TM}{}_{np}\frac{nk_z}{\rho}J_n(\frac{x_{np}}{a}\rho)\cos n\phi & TM_{np}^o \end{cases}$$

$$E_z = e^{jk_z z}\begin{cases} 0 & TE_{np}^e \\ 0 & TE_{np}^o \\ -jN_{np}^{TM}(\frac{x_{np}}{a})^2 J_n(\frac{x_{np}}{a}\rho)\cos n\phi & TM_{np}^e \\ -jN_{np}^{TM}(\frac{x_{np}}{a})^2 J_n(\frac{x_{np}}{a}\rho)\sin n\phi & TM_{np}^o \end{cases}$$

In these, J_n and J'_n denote the nth order Bessel function and its derivative respectively, x_{np} and x'_{np} are their p'th roots, a is the radius of the cylindrical guide and k_z denotes the propagation constant of each mode given by

$$k_z = \begin{cases} \sqrt{k^2 - \left(\frac{x'_{np}}{a}\right)^2} & TE \\ \sqrt{k^2 - \left(\frac{x_{np}}{a}\right)^2} & TM \end{cases}$$

The superscripts (e/o) denote the even or odd phi dependance of the field. The index m compatcly represents all of the TE^e_{np}, TE^o_{np}, TM^e_{np}, and TM^o_{np} modes. The mode normalization constants N^{TE}_{np} and N^{TM}_{np} are defined so that all modes have unity power and are given by [10].

$$N^{TM}_{np} = \left[\frac{1}{2}J'_n(x_{np})\, x_{np}\sqrt{\pi k Y k_z \varepsilon_n}\right]^{-1}$$

$$N^{TE}_{np} = \left[\frac{1}{2}J_n(x'_{np})\sqrt{\pi k Z k_z \varepsilon_n \{\left(\frac{x'_{np}}{a}\right)^2 - a^2\}}\right]^{-1}$$

$$\varepsilon_n = \begin{cases} 2 & n = 0 \\ 1 & n \neq 0 \end{cases}$$

where $Z = \frac{1}{Y}$ being the intrinsic free space impedance and k is the free space wave number.

References

[1]P. P. Silvester and R. L. Ferrari, *Finite Elements for Electrical Engineers*, Cambridge, 1986.

[2]J. L. Volakis, A. Chaterjee and L. C. Kempel, "A review of the finite element method for three-dimensional electromagnetic scattering." *J. Opt. Soc. Am.-A*, April 1994 (to appear)

[3]D. C. Ross, J. L. Volakis and T. Ozdemir, "A New Finite Element Formulation for Modeling Circular Inlets with Irregular Terminations", Technical Report 030395-1-T, The University of Michigan, EECS Radiation Laboratory, Ann Arbor MI, May 1993.

[4]H. Ling, R. Chou and S. W. Lee, "Shooting and Bouncing Rays: Calculating the RCS of an Arbitrary Shaped Cavity", *IEEE Transactions on Antennas and Propagation*, vol. AP-37, no. 2, pp 194-205, Feb. 1989.

[5]P. H. Pathak and R. J. Burkholder, "High Frequency EM Scattering by Open-Ended Waveguide Cavities", *Radio Science*, vol. 26, no. 1, pp. 211-218, Jan.-Feb. 1991.

[6]A. Altintas, P. H. Pathak and M. C. Liang, "A Selective Modal Scheme for the Analysis of EM Coupling into or Radiation from Large Open-ended Waveguides", *IEEE Transactions on Antennas and Propagation,* vol. AP-36, no. 1, pp. 84-96, Jan. 1988.

[7]H. T. Anastassiu and J. L. Volakis, "The Mode Matching Technique for Electromagnetic Scattering by Inlets with Complex Terminations", Technical Report 030395-3-T, The University of Michigan, EECS Radiation Laboratory, Ann Arbor MI, October 1993.

[8]Ching-Chao Huang, "Ray Analysis of EM Backscatter from a Cavity Configuration", Ph.D. Dissertation, The Ohio State University, ElectroScience Laboratory, Columbus OH, 1982.

[9]P. Y. Ufimtsef, "Method of Edge Waves in the Physical Theory of Diffraction" (in Russian) *Izd-Vo Sov. Radio,* pp. 1-243, 1962. (English Translation, U.S. Air Force Foreign Technology Division, Wright-Patterson Air Force Base, Dayton OH, 1971).

[10]P. H. Pathak, C. W. Chuang, M. C. Liang, "Inlet Modeling Studies", Technical Report 717674-1, The Ohio State University, ElectroScience Laboratory, Columbus OH, October 1980.

[11]P. H. Pathak and R. J. Burkholder, "A Reciprocity Formulation for the EM Scattering by an Obstacle Within a Large Open Cavity", *IEEE Transactions on Microwave Theory and Techniques*, vol. MTT-41, no. 4, pp. 702-707, Apr. 1993.

[12]D. C. Ross, "Some Finite-Element Preprocessing Algorithms for Electromagnetic Scattering", I*EEE Antennas and Propagation Magazine*, Vol. 35, No. 3, pp. 68-72, June 1993.

[13]K. D. Paulsen, D. R. Lynch and J. W. Strohbehn, "Three-dimensional finite, boundary and hybrid element solutions of the Maxwell equations for lossy dielectric media," *IEEE Trans. Microwave Theory Tech.*, vol. 36, no. 4, pp 682-693, Apr. 1988.

[14]M. L. Barton and Z. J. Cendes, "New vector finite elements for three-dimensional magnetic field computation", *J. Appl. Phys.*, vol. 61, no. 8, pp. 3919-3921, Apr. 1987.

[15]Z. J. Cendes, "Vector Finite Elements for Electromagnetic Field Computation", *IEEE Trans. on Magnetics*, Vol. 27, No. 5, pp. 3953-3966, Sept. 1991.

[16]B. M. Azizur Rahman and J. B. Davies, "Penalty Function Improvement of Waveguide Solutions by Finite Elements", *EEE Trans. Microwave Theory Tech.*, vol. 32, no. 8, pp 922-928, Aug. 1984.

[17]A. B. MacFarland, "Parameter Centering and Tolerancing", Master's Thesis, Electrical Engineering Graduate School, Univ. of Idaho, Aug. 86.